Cancer Cell
Article

A Small Molecule Inhibitor of Ubiquitin-Specific Protease-7 Induces Apoptosis in Multiple Myeloma Cells and Overcomes Bortezomib Resistance

Dharminder Chauhan,[1,9,*] Ze Tian,[1,9] Benjamin Nicholson,[2] K.G. Suresh Kumar,[2] Bin Zhou,[3] Ruben Carrasco,[1] Jeffrey L. McDermott,[2] Craig A. Leach,[2] Mariaterresa Fulcinniti,[1] Matthew P. Kodrasov,[2] Joseph Weinstock,[2] William D. Kingsbury,[2] Teru Hideshima,[1] Parantu K. Shah,[1] Stephane Minvielle,[4] Mikael Altun,[5] Benedikt M. Kessler,[6] Robert Orlowski,[7] Paul Richardson,[1] Nikhil Munshi,[1,8] and Kenneth C. Anderson[1,*]

[1]Department of Medical Oncology, The LeBow Institute for Myeloma Therapeutics and Jerome Lipper Myeloma Center, Dana Farber Cancer Institute, Harvard Medical School, Boston, MA 02215, USA
[2]Progenra, Inc., Malvern, PA 19355, USA
[3]Institute for Nutritional Sciences, Shanghai Institute for Biological Sciences, Chinese Academy of Sciences, Shanghai, China 200031
[4]Inserm U892, Universite de Nantes, 44200 Nantes, France
[5]Department of Medical Biochemistry and Biophysics, Karolinska Institute, 171 77 Stockholm, Sweden
[6]Nuffield Department of Medicine, University of Oxford, Roosevelt Drive, Oxford OX3 7BN, UK
[7]Department of Lymphoma and Myeloma, The University of Texas M.D. Anderson Cancer Center, Houston, TX 77030, USA
[8]Veterans Administration Boston Healthcare System, Boston, MA 02115, USA
[9]These authors contributed equally to this work
*Correspondence: dharminder_chauhan@dfci.harvard.edu (D.C.), kenneth_anderson@dfci.harvard.edu (K.C.A.)
http://dx.doi.org/10.1016/j.ccr.2012.08.007

SUMMARY

Bortezomib therapy has proven successful for the treatment of relapsed/refractory, relapsed, and newly diagnosed multiple myeloma (MM); however, dose-limiting toxicities and the development of resistance limit its long-term utility. Here, we show that P5091 is an inhibitor of deubiquitylating enzyme USP7, which induces apoptosis in MM cells resistant to conventional and bortezomib therapies. Biochemical and genetic studies show that blockade of HDM2 and p21 abrogates P5091-induced cytotoxicity. In animal tumor model studies, P5091 is well tolerated, inhibits tumor growth, and prolongs survival. Combining P5091 with lenalidomide, HDAC inhibitor SAHA, or dexamethasone triggers synergistic anti-MM activity. Our preclinical study therefore supports clinical evaluation of USP7 inhibitor, alone or in combination, as a potential MM therapy.

INTRODUCTION

Normal cellular homeostasis is maintained by a balanced regulation of protein synthesis and degradation. The ubiquitin proteasome system (UPS) is a nonlysosomal intracellular protein degradation pathway mediated via proteasome holoenzyme, ubiquitin ligases, and deubiquitylating (DUB) enzymes (Hershko, 2005). Specifically, the covalent attachment of ubiquitin to target substrates leads to protein degradation via the multicatalytic 26S proteasome complex (Adams, 2004; Ciechanover, 2005); conversely, the ubiquitylation process can be reversed by DUBs, which specifically cleave the isopeptide bond at the C terminus of Ub (Nicholson et al., 2008). Deregulation of the UPS pathway is linked to the pathogenesis of various human diseases (Adams, 2004; Hoeller et al., 2006); therefore, inhibitors of the UPS pathways, either at the level of proteasome, ubiquitylating, or DUB enzymes offers great promise as a novel therapeutic strategy.

Indeed, preclinical and clinical studies provided the basis for FDA approval of the first-in-class proteasome inhibitor bortezomib for treatment of multiple myeloma (MM) (Richardson et al., 2003). Even though bortezomib therapy is a major advance, it

Significance

Deregulation of the ubiquitin-proteasome system (UPS) is linked to pathogenesis of various human diseases, including cancer. Targeting the proteasome has proven to be a successful therapy in multiple myeloma (MM) patients. Recent research efforts led to the discovery of newer agents that target enzymes modulating protein ubiquitin-conjugation/deconjugation rather than the proteasome itself, with the goal of generating more specific and less toxic antitumor agents. Here, we utilized both in vitro and in vivo MM xenograft models to show antitumor efficacy of a small molecule inhibitor of ubiquitin-specific protease-7 (USP7) P5091. Our preclinical data showing efficacy of P5091 in MM disease models provides the framework for clinical evaluation of USP7 inhibitors to improve patient outcome in MM.

has been associated with possible off-target toxicities and the development of drug-resistance (Lonial et al., 2005). More recent efforts have focused on the discovery and development of small molecule inhibitors of other major components of UPS, including inhibitors of DUBs, E1-conjugating enzyme, or E3 ubiquitin ligase. Among these, DUBs have emerged as a potential therapeutic target, given their role in several human diseases (Nicholson et al., 2007).

USP7 regulates key biological signaling pathways in tumorigenesis (Everett et al., 1997; Hu et al., 2002; Li et al., 2002; Nicholson et al., 2007), and its overexpression in prostate cancer correlates with tumor aggressiveness (Song et al., 2008). *MDM2*, a murine double minute oncogene (human ortholog *HDM2*), is a primary substrate of USP7 and negatively regulates the tumor suppressor protein p53 (Cummins et al., 2004; Li et al., 2004). MDM2 ubiquitylates p53 and targets it for proteasome-mediated degradation. Under normal conditions USP7 stabilizes MDM2 levels, which consequently drives p53 ubiquitylation and subsequent degradation. Although MDM2 has autoubiquitylase activity (Fang et al., 2000; Stommel and Wahl, 2004) and a short half-life, which can be abrogated by USP7, a more recent in vivo knockin model of inactive *MDM2* showed that it is still efficiently ubiquitylated through self-ubiquitylation-independent mechanisms (Itahana et al., 2007). Genetic ablation of *USP7* using siRNA or somatic knockout (KO) prevents USP7 from deubiquitylating MDM2, resulting in stabilization of p53 (Cummins et al., 2004; Kon et al., 2010; Li et al., 2004; Meulmeester et al., 2005). Furthermore, p53 protein levels were elevated in $USP7^{-/-}$embryos, and the embryonic lethality of $USP7^{-/-}$ mice was delayed in a $p53^{-/-}$ background (Kon et al., 2010). The functional consequences of inhibiting USP7 therefore include decreased HDM2 levels with accumulation of p53, induction of growth arrest via p21, and cell death. Mutations or deletions of p53 are late events in MM, and activation of p53 may offer a novel therapeutic strategy (Anderson, 2007). USP7 also deubiquitylates other cancer targets (PTEN, FOXO4, or claspin) and plays a role in DNA replication, apoptosis, and endosomal organization (Nicholson et al., 2007). Therapeutic strategies using USP7 inhibitors allow for specific targeting of the UPS and are therefore less likely to trigger off-target activities and associated toxicities.

Here, we demonstrate the efficacy of a small molecule inhibitor of USP7 P5091 in MM using both in vitro and in vivo models. These findings provide the proof-of-concept for evaluation of USP7 inhibitors as anti-MM agents.

RESULTS AND DISCUSSION

P5091 Is a Selective Inhibitor of USP7

P5091 is a trisubstituted thiophene with dichlorophenylthio, nitro, and acetyl substituents mediating anti-USP7 activity (Figure 1A). P5091 was discovered using a ubiquitin-phospholipase A_2 enzyme (Ub-PLA_2) reporter assay (Figure 1B) in a high-throughput screening for inhibitors of USP7 from a diversity-based library of small molecules. The structure-activity relationship (SAR) data for selected analogs of P5091 is shown in Figure 1C. Comparison of the halogen substituents of the 5-arylsulfanyl moiety of the 2-acetyl-4-nitro-5-arylsulfanylthiophenes demonstrated that the unsubstituted phenyl analog 1 was not active as a USP7 antagonist, whereas all of the 5- mono and dihalo phenylsulfanylthiophenes, including P5091 (5), exhibited USP7 inhibitory activity. In addition, the dichloro analogs (5–7) and difluoro analog were more potent than the monochloro analogs (2–4). Initial exploration of the R2 position (9–12) did not result in enhanced potency. Importantly, P5091 (Compound 5; Figure 1C) exhibited potent, specific, and selective deubiquitylating activity against USP7 (EC_{50} = 4.2 ± 0.9 μM). In contrast, P5091 did not inhibit other DUBs or other families of cysteine proteases tested (EC_{50} > 100 μM) (Figure 1D). P22074, an inactive analog of P5091, served as a negative control (Figure 1D).

To determine the USP7 inhibitory activity of P5091 in living cells, we performed competition assays between P5091 and the ubiquitin (Ub) active site probe Ub-vinyl methyl ester (HA-UbVME) (Borodovsky et al., 2002). P5091 inhibited the labeling of USP7 with HA-UbVME in a concentration-dependent manner (Figure 1E). Untreated cell lysates incubated with Ub-probes exhibited Ub-USP7 conjugate formation, as reflected by the increase in mass of USP7 of ~10 kDa. In contrast, Ub-USP7 conjugate formation was inhibited in cell lysates from P5091-treated cells at concentrations as low as 5–10 μM P5091, with a concomitant increase in the unlabeled free form of USP7. No gross difference in the labeling of other DUBs with Ub-VME was observed, even at 40 μM. The residual active USP7 may relate to the irreversibility-related potency of HA-Ub probe versus P5091 and/or kinetics of labeling of HA-Ub probe against USP7. P5091 treatment did not inhibit other DUBs, such as USP5, UCHL1, or UCHL3 (Figure S1A available online). These data demonstrate the P5091 activity against USP7 in the cellular environment.

Isopeptidase activity analyses shows that USP7 efficiently cleaves high molecular weight polyubiquitin chains (Ub7- and K48-linked ubiquitin chains), and USP7-mediated cleavage of these chains is inhibited in a dose-dependent manner by P5091 (Figure 1F). Moreover, P5091 inhibits USP7- but not USP2- or USP8-mediated cleavage of poly K48-linked ubiquitin chains (visualized by the presence or absence of monoubiquitin) (Figure S1B).

USP7 Knockout Renders Cells Resistant to P5091

To further determine whether the inhibitory effect of P5091 is mediated via USP7, we utilized human cells (HCT116 $USP7^{-/-}$) in which the *USP7* is disrupted by targeted homologous recombination (Cummins et al., 2004). P5091 decreased the viability of HCT116 (WT) cells in a time- and concentration-dependent manner; conversely, a marked reduction in P5091 cytotoxic activity was observed against HCT116 $USP7^{-/-}$ cells (Figure 1G). HCT116 $USP7^{-/-}$ cells are slow proliferating cells compared to HCT116 (WT). To exclude the possibility that the differences observed during P5091 treatment is not due to growth rate, cells were serum starved and examined for P5091 effects. In agreement with our results in Figure 1G, P5091 decreased the viability of HCT116 (WT) cells, whereas cytotoxic activity of P5091 was significantly blocked in $USP7^{-/-}$ cells (Figure S1C). $USP7^{-/-}$ mice die during early embryonic development (Kon et al., 2010). The KO selection process in HCT116 $USP7^{-/-}$ cells can contribute to the development of a compensatory mechanism for the loss of USP7 for survival. Nonetheless, our data using HCT116 $USP7^{-/-}$ cells suggests that P5091 targets USP7.

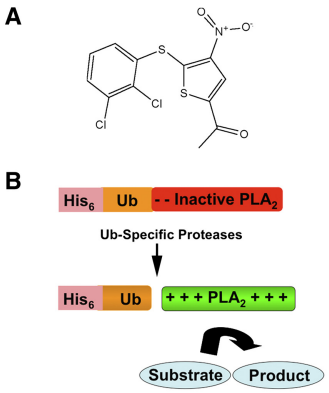

C

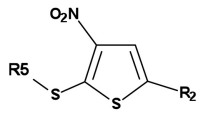

Compound #	R2	R5	USP7 inhibition EC_{50} (μM)
1	Acetyl	phenyl	>50
2	Acetyl	2-chlorophenyl	12.9 ± 4.3
3	Acetyl	3-chlorophenyl	7.0 ± 2.1
4	Acetyl	4-chlorophenyl	11.8 ± 3.0
5	Acetyl	2,3-dichlorophenyl	4.2 ± 0.9
6	Acetyl	3,5-dichlorophenyl	6.4 ± 1.4
7	Acetyl	2,4-dichlorophenyl	6.5 ± 2.6
8	Acetyl	2,4-difluorophenyl	8.0 ± 2.8
9	1-hydroxyethyl	2,4-dichlorophenyl	20.1 ± 4.3
10	Ethyl	2,3-dichlorophenyl	>50
11	n-butyl	2,4-dichlorophenyl	13.9 ± 4.2

D

Enzyme	EC_{50} (μM)	
	P5091	P22074
USP2c	>100	>100
USP5	>100	>100
USP7	4.2±0.9	>100
USP8c	>100	>100
USP15	>100	>100
USP20	>100	>100
USP21	>100	>100
USP28	>100	>100
UCH-L1	>100	>100
Caspase 3	>100	>100
Cathepsin K	>100	>100
Calpain 1	>100	>100
MMP13	>100	>100
Cathepsin D	>100	>100
EK_L	>100	>100
PLA_2	>100	>100

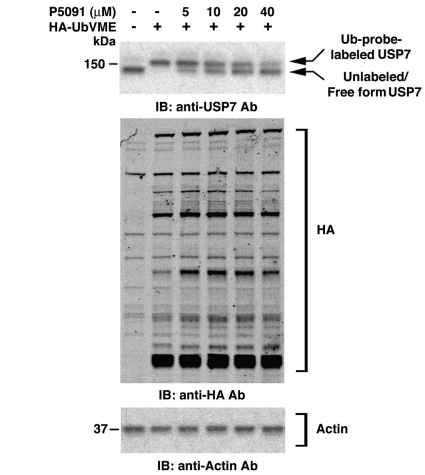

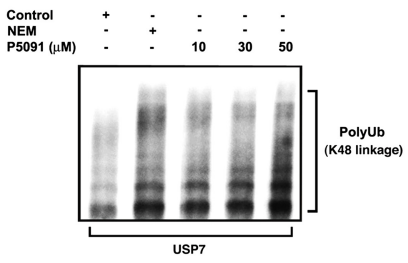

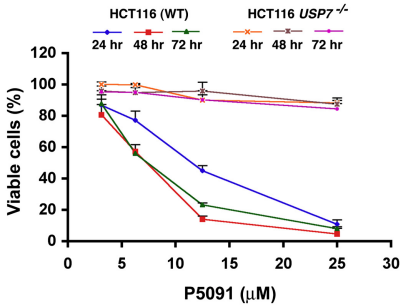

Figure 1. P5091 Is a Selective Inhibitor of USP7 Activity

(A) Chemical structure of P5091.

(B) Schematic representation of Ub-PLA_2 isopeptidase reporter assay: cleavage by the isopeptidase at the carboxy-terminal glycine of the Ub releases catalytically active PLA_2, which liberate a quantifiable fluorescent product in the presence of its substrate.

(C) Structure-activity relationship data for selected analogs of P5091 (compound 1 = P22074 and compound 5 = P5091).

(D) P5091 demonstrates potent and specific inhibition of USP7 in vitro versus other DUBs and proteases.

(E) HEK293T cells were treated with DMSO or P5091; crude cell extracts were labeled with indicated UbVME probe, followed by immunoblotting (IB) with indicated antibodies.

(F) P5091 inhibits higher molecular weight polyubiquitin chain cleavage in a dose-dependent manner. NEM (N-ethyl maleimide) is a nonspecific inhibitor of USP7 and served as control.

(G) HCT116 (WT) and HCT116 *USP7*$^{-/-}$ cells were treated with vehicle or indicated concentrations of P5091 for 24, 48, and 72 hr and then analyzed for viability using MTT assay (mean ± SD; n = 3). Error bars indicate SD.

See also Figure S1.

P5091 Targets USP7 Substrate HDM2

Genetic ablation of USP7 destabilizes its substrate, HDM2 (Cummins et al., 2004; Li et al., 2004). U20S cells were transiently transfected with HA-Ub constructs, and endogenous HDM2 ubiquitylation was analyzed by pulling down ubiquitylated proteins using Tandem Ubiquitin Binding Entities (TUBEs) (Hjerpe et al., 2009). Empty-vector/vehicle served as a control to determine the effects of HA-Ub alone on HDM2 ubiquitination (Figure 2A, lane 2, empty vector versus lane 3, HA-Ub). HA-Ub transfection alone slightly increases HDM2-ubiquitination versus empty-vector. Importantly, addition of P5091 markedly increases HDM2 ubiquitination, in particular, the band between 130–170 (lane 3 versus lane 4). The band between 130–170 kDa likely represents a predominantly multiubiquitylated form of HDM2; a similar banding pattern has been recently reported (Zhao et al., 2011). The mock pulldown (lane 1) is negative control for TUBE1 using unconjugated Agarose. Alternatively, we asked whether HDM2 stabilization is affected in the presence of P5091. P5091 accelerates the degradation of HDM2 versus control cycloheximide (CHX) alone-treated U20S cells (Figure 2B). Likewise, P5091 enhanced the degradation of HDM2 in prostate cancer cell lines (Figure S2). Together, our data suggest that USP7 inhibition by P5091 induces HDM2 polyubiquitylation and accelerates degradation of HDM2.

Prognostic relevance of USP7 in multiple myeloma proteasome inhibition has proven to be a successful treatment strategy for MM patients (Richardson et al., 2003). Because USP7 is also a component of UPS, we examined the effects of USP7 inhibition with P5091 in MM cells. Immunohistochemistry (IHC) studies using bone marrow (BM) biopsies from MM patients and normal healthy donors showed a significantly higher *USP7* expression in MM cells than in normal cells (Figure 3A). Normal plasma cells lack detectable *USP7* expression. Similar results were observed using protein extracts from MM patient tumor cells versus normal cells, and MM cell lines (Figure 3B).

We retrospectively analyzed the prognostic significance of baseline USP7 expression from BM biopsy samples on the

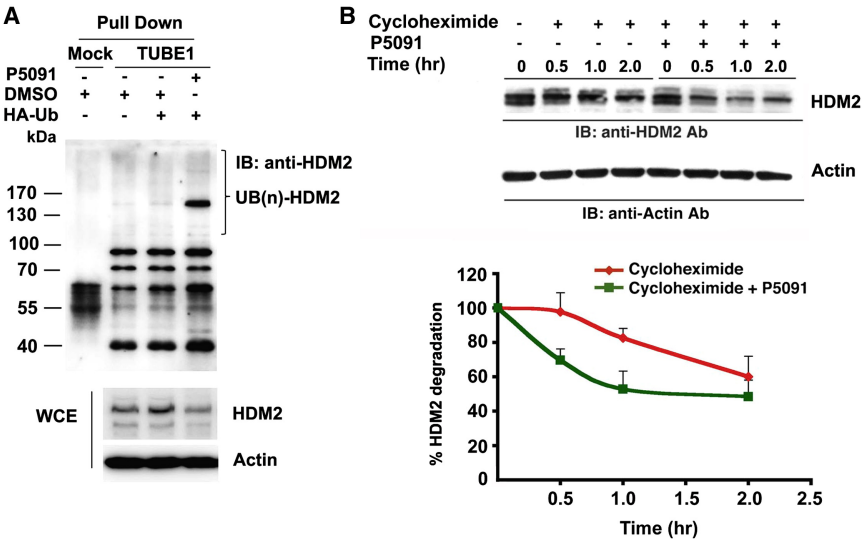

Figure 2. Effect of P5091 on USP7 Substrate HDM2

(A) U2OS cells were transfected with HA-Ub (WT), and 48 hr posttransfection, cells were treated with DMSO or P5091 (30 μM) for 4 hr. Endogenous HDM2 ubiquitylation was analyzed by pulling down ubiquitylated proteins using TUBEs (Supplemental Experimental Procedures). Cell lysates were normalized for HDM2 protein and incubated with uncojugated Agarose or TUBE1 conjugated Agarose; samples were separated by SDS-PAGE, and HDM2 ubiquitylation was detected using anti-HDM2 antibody. Whole-cell extracts (WCE) were subjected to IB using anti-HDM2 and anti-actin antibodies.

(B) U2OS cells were pretreated with either vehicle or P5091 (15 μM, IC_{50}) for 2.0–3.5 hr, followed by addition of CHX (40 μg/ml) for the indicated times. Total proteins lysates were subjected to immunoblotting with anti-HDM2 or anti-actin antibodies. Densitometry was utilized to quantify HDM2 protein levels after normalization with actin control to obtain percent HDM2 degradation (mean ± SD; n = 3).

Error bars indicate SD. See also Figure S2.

overall survival and event-free survival of 170 MM patients enrolled in a clinical trial. Results show a statistically significant inverse correlation between USP7 levels and overall survival (Figure 3C). Additionally, MM patients with lower USP7 levels survived for longer timespan with no recurrence of the disease following therapy (Figure 3D). Together, these data suggest a role of USP7 in the pathogenesis of MM and provide a rationale for targeting USP7 in MM.

P5091 Inhibits USP7 Deubiquitylating Activity, without Blocking Proteasome Activity, in MM Cells

P5091 causes significant inhibition (>50%) of USP7 activity in a concentration-dependent manner (Figure 4A). Although bortezomib blocks chymotrypsin-like (CT-L) proteasome activity, no significant inhibition of CT-L activity was observed in P5091-treated MM cells (Figure 4B). P5091 (25–50 μM) had no effect on trypsin-like (T-L)- or caspase-like (C-L) proteasome activities (Figure S3A). A comparative analysis shows that bortezomib induced a marked increase in ubiquitylated proteins (Figure 4B), whereas a modest increase in polyubiquitylation was observed in P5091-treated cells. This is likely due to the narrow USP7 substrate activity compared to bortezomib, which has a broader substrate spectrum. These data suggest that P5091 blocks USP7 activity without altering proteasome function.

P5091 Inhibits Growth in MM Cells and Overcomes Bortezomib-Resistance

P5091 induces a dose-dependent decrease in viability of various MM cell lines, including those that are resistant to conventional therapies dexamethasone (Dex) (MM.1R), doxorubicin (Dox-40), or melphalan (LR5) (IC_{50} range 6–14 μM) (Figure 4C). P5091 blocks the USP7 activity in MM at the IC_{50} of P5091 for these cells (Figure 4A and data not shown). In contrast, P22074 had no significant effect on the viability. The variable IC_{50} of P5091 against MM cell lines may be due to their distinct genetic background and/or drug-resistance characteristics (Anderson, 2007). USP7-siRNA inhibited cell proliferation; conversely, transfection of USP7 (WT) rescued cells from the growth-inhibitory effects of USP7-siRNA (Figure 4D). Immunoblot analysis shows a significant knockdown of USP7 by USP7-siRNA versus scrambled (scr)-siRNA, and restoration of USP7 levels in cells transfected with USP7 (WT) versus USP7-siRNA (Figure 4D, inset).

To determine whether P5091 similarly affects purified patient MM cells, tumor cells from eight MM patients, including those relapsing after multiple prior therapies, such as bortezomib, lenalidomide, and Dex, were treated with P5091. Patient MM was deemed to be refractory to bortezomib therapy when progressive disease occurred in spite of bortezomib treatment; in addition, most bortezomib-resistant MM was refractory to lenalidomide and Dex therapies as well. A dose-dependent decrease in the viability of all patient MM cells was noted after P5091 treatment (Figure 4E). We next examined whether tumor cells from bortezomib-resistant MM patients are affected by bortezomib treatment in vitro and whether P5091 exerts a cytotoxic effect in these cells (Figure 4F). Results demonstrate a varying sensitivity to bortezomib in vitro (10%–50% decrease in viability), albeit at much higher concentrations (12.5 nM) than normally observed IC_{50} for MM cells (3–5 nM) in three of six samples; however, all patient cells were significantly more sensitive to P5091 ($IC_{50} \leq 3$ μM). These findings show the ability of P5091 to trigger cytotoxicity, even in patient tumor cells resistant to bortezomib, Dex, or lenalidomide therapies.

To further address this issue, we utilized bortezomib-sensitive (ANBL-6.WT) and bortezomib-resistant (ANBL-6.BR) isogenic MM cell lines. Cell viability analysis showed that the IC_{50} of drugs for ANBL-6.WT or ANBL-6.BR were 2.32 nM and 12.05 nM for bortezomib and 6.83 μM and 9.85 μM for P5091. As seen in Figure 4G, the IC_{50} ratio (ANBL-6.BR/ANBL-6.WT) of P5091 is significantly less than bortezomib ($p < 0.001$), demonstrating the ability of P5091 to overcome bortezomib resistance. Finally, P5091 at the IC_{50} for MM cells does not significantly affect the

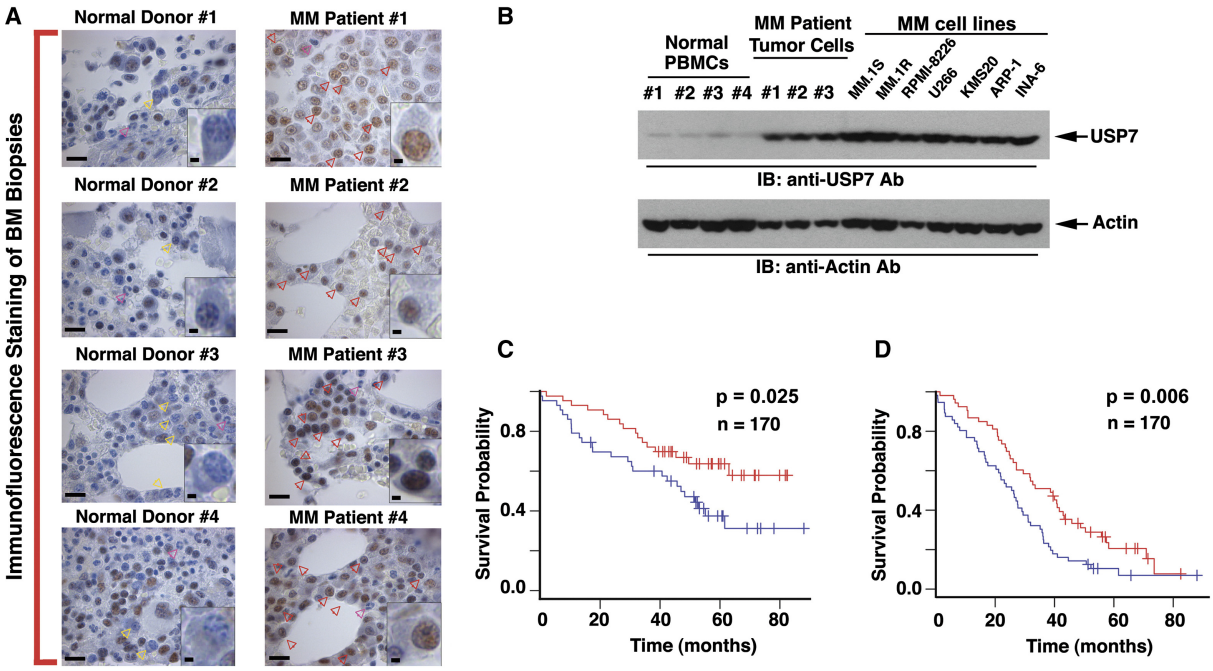

Figure 3. USP7 Expression and Prognostic Relevance in MM Cells

(A) IHC analysis of BM biopsies from normal donors and MM patients to show USP7 expression. Red arrowheads indicate USP7-positive cells (brown color). Yellow arrowheads represent normal plasma cells; magenta arrowheads are neutrophils. Scale bars, 50 μm (10 μm in insets).

(B) Purified tumor cells from MM patients, normal peripheral blood mononuclear cells (PBMCs), and MM cell lines were analyzed for USP7 expression level by IB with anti-USP7 and anti-actin antibodies.

(C and D) Kaplan-Meier plots on prognostic relevance of *USP7* expression on the overall and event-free survival for MM patients. The blue line indicates a patient group with higher *USP7* expression and shorter survival, whereas the red line represents a group of patients with lower *USP7* expression and longer survival. See Web site (http://www.ncbi.nlm.nih.gov/geo/) for gene expression data under accession number GSE39754.

viability of normal PBMCs (Figure 4H). Higher concentrations of P5091 (25 μM) decrease the viability of PBMCs by 20%–25%, suggesting that normal cells are not completely refractory to P5091. These data show a favorable therapeutic index for P5091 in MM.

P5091 Overcomes Bone Marrow Stromal Cell-Induced Growth of MM Cells

Interaction of MM cells with BMSCs triggers cytokine secretion, which mediates paracrine growth of MM cells and protects against drug-induced apoptosis (Chauhan et al., 2005b). To determine whether P5091 affects BMSCs-triggered MM cell growth, MM.1S cells were cultured with or without BMSCs in the presence or absence of various concentrations of P5091. P5091 treatment inhibited BMSCs-induced proliferation of MM.1S (Figure 4I). P5091 treatment does not affect the viability, morphology, or function of BMSCs (Figures S3B–S3D). These data suggest that P5091 not only directly targets MM cells but also overcomes the cytoprotective effects of the MM-host BM microenvironment.

We next examined whether anti-MM activity of P5091 is due to apoptosis. P5091 treatment shows accumulation of cells in early- (Ann V^+/PI^-) and late-stage (Ann V^+/PI^+) apoptosis (Figure S3E), associated with proteolytic cleavage of poly (ADP) ribose polymerase (PARP) (Figure S3F). Treatment of MM.1S and RPMI-8226 cells with P5091 induces caspase-3 cleavage and activates caspase-9 and casapse-8 apoptotic pathways (Figure S3F). Biochemical inhibition of either caspase-8 (IETD-FMK) or pan-caspase inhibitor (Z-VAD-FMK) markedly abrogates P5091-triggered cytotoxicity (Figure 4J). These findings suggest that (1) P5091 triggers both mitochondria-dependent and mitochondria-independent signaling pathways and (2) P5091-induced apoptosis is mediated, at least in part, via caspases.

Effect of P5091 on HDM2/p53/p21 Pathway in MM Cells

In agreement with our results using U20S cells (Figure 2A), P5091 increases ubiquitination of endogenous HDM2 in MM.1S cells (Figure S4A). In contrast to U20S cells, higher levels of endogenous poly-Ub HDM2 were observed in MM.1S cells in the absence of exogenous Ub transfection. Importantly, a significant increase in HDM2 ubiquitination was noted in P5091-treated cells compared to untreated cells. Even though similar bands are observed in DMSO-treated U2OS cells (Figure 2A, lanes 2 and 3) as well as in MM.1S cells (Figure S4A), P5091 treatment resulted in accumulation of band between 130–170 kDa only in U2OS cells (Figure 2A, lane 3), suggesting cell-type-specific differences in HDM2 ubiquitination that is sensitive to P5091 treatment.

USP7 regulates HDM2, HDMX, and p53 pathways (Cummins et al., 2004; Li et al., 2004). P5091 decreased HDM2 and HDMX, as well as upregulated p53 and p21 levels (Figure 5A). Pretreatment of MM.1S cells with P5091, followed by CHX

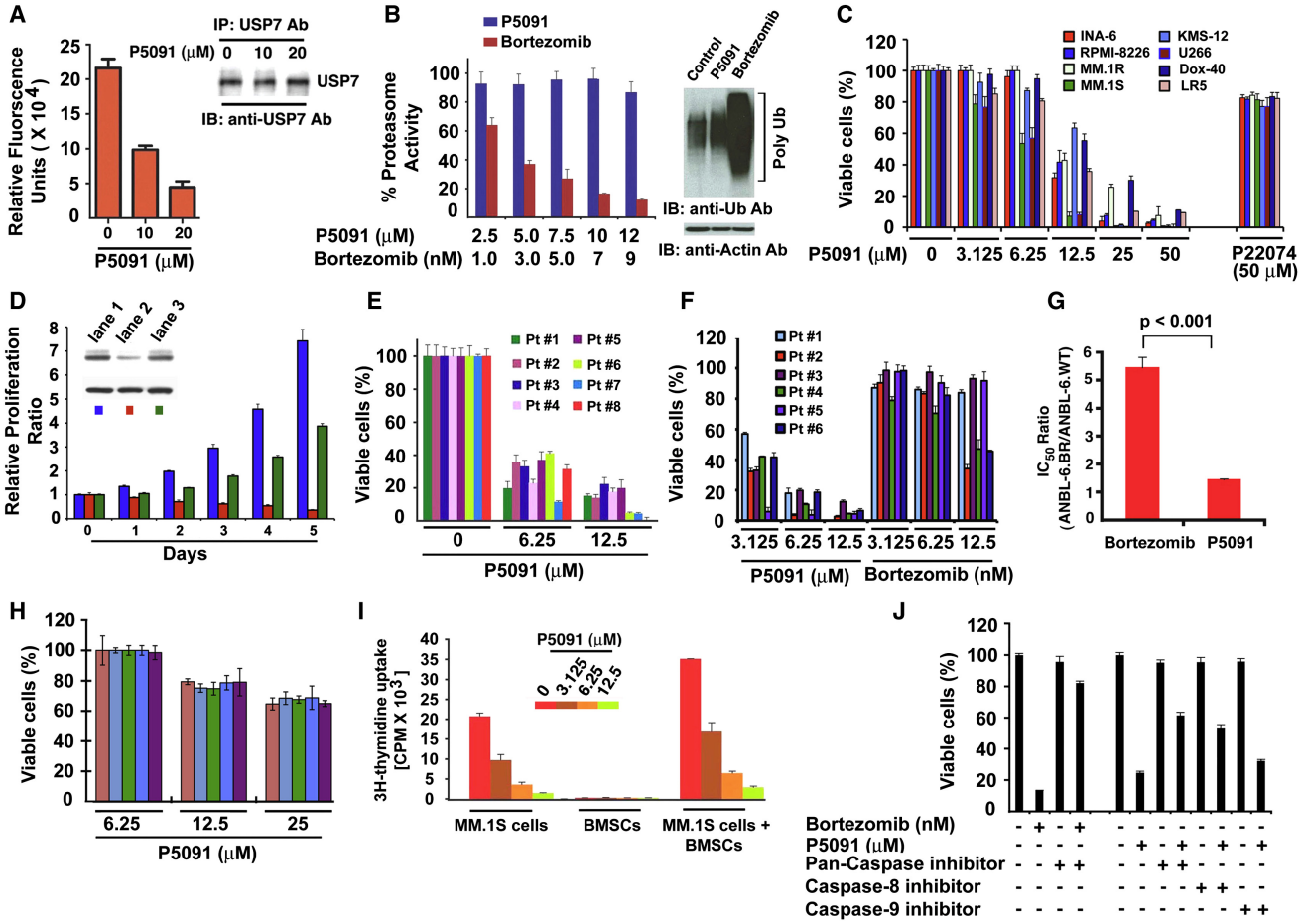

Figure 4. P5091 Inhibits USP7 Activity, Induces MM Cell Death, and Overcomes Bortezomib-Resistance

(A) MM.1S cells were treated with DMSO or with P5091 for 3 hr; cellular USP7 was immunoprecipitated under native conditions and analyzed for USP7 activity using the Ub-EK$_L$ assay ($p < 0.05$; n = 2).

(B) MM.1S cells were treated with DMSO or with P5091 or bortezomib for 3 hr; protein lysates were analyzed for proteasome activity. Raw data were normalized to percent proteasome activity in control (as 100%) versus drug-treated cells (mean ± SD; n = 3). Protein lysates from control, P5091-, or bortezomib-treated MM.1S cells were subjected to IB with anti-Ub antibody.

(C) MM cell lines were treated with DMSO or with P5091 for 48 hr, followed by assessment for cell viability (mean ± SD; $p < 0.001$ for all cell lines; n = 3).

(D) MM.1S cells were cotransfected with scr-siRNA plus empty-vector, USP7-siRNA plus empty-vector, or USP7-siRNA plus active USP7 (WT) and subjected to growth analysis using CellTiter-Glo assay (mean ± SD; n = 3). Immunoblot shows USP7 expression in cells transfected with scr-siRNA plus empty-vector (lane 1), USP7-siRNA plus empty-vector (lane 2), or USP7-siRNA plus active USP7 (WT) (lane 3) (Inset).

(E) Purified patient MM cells were treated with P5091 for 48 hr and analyzed for viability (mean ± SD of triplicate cultures; $p < 0.001$ for all patient samples).

(F) MM cells from six bortezomib-resistant patients (Pt. #1–#6) were treated in a side-by-side manner with either bortezomib or P5091 for 48 hr and analyzed for viability (mean ± SD of triplicate cultures; $p < 0.001$ for all patient samples).

(G) Bortezomib-sensitive (ANBL-6.WT) and Bortezomib-resistant (ANBL-6.BR) cells were treated with either bortezomib or P5091 for 48 hr, followed by assessment for cell viability. The bar graph shows the IC$_{50}$ ratio (ANBL-6.BR/ANBL-6.WT) of P5091 and bortezomib (mean ± SD; n = 2).

(H) Normal PBMCs were treated with P5091 for 48 hr and analyzed for viability (mean ± SD of quadruplicate cultures).

(I) MM.1S cells were cultured with or without BMSCs for 72 hr, and DNA synthesis was measured by ^{3}H-TdR uptake (mean ± SD of triplicate cultures; $p < 0.001$ for all samples).

(J) MM.1S cells were pretreated with inhibitors of caspase-8, caspase-9, or pan-caspase for 1 hr, and then P5091 (12.5 μM) or bortezomib (10 nM) was added for another 24 hr, followed by analysis of viability.

Error bars (A–J) indicate SD. See also Figure S3.

addition resulted in the rapid degradation of HDM2 and increased steady-state protein levels of p53 and p21 (Figure 5B). This increase in p53 and p21 was not due to enhanced transcription at the tested time point (Figure S4B). HDMX stability was only slightly decreased in both control and P5091-treated cells, likely because of its long half-life in human cancer cells (Li and Gu, 2011). The P5091-induced HDM2 degradation was blocked in the presence of proteasome inhibitor MG132 (Figure S4C), suggesting that HDM2 degradation is proteasome dependent.

We next examined the role of HDM2, p53, and p21 during P5091-induced cytotoxicity using loss-of-function studies and a KO cell system. HDM2-siRNA reduced HDM2 levels compared

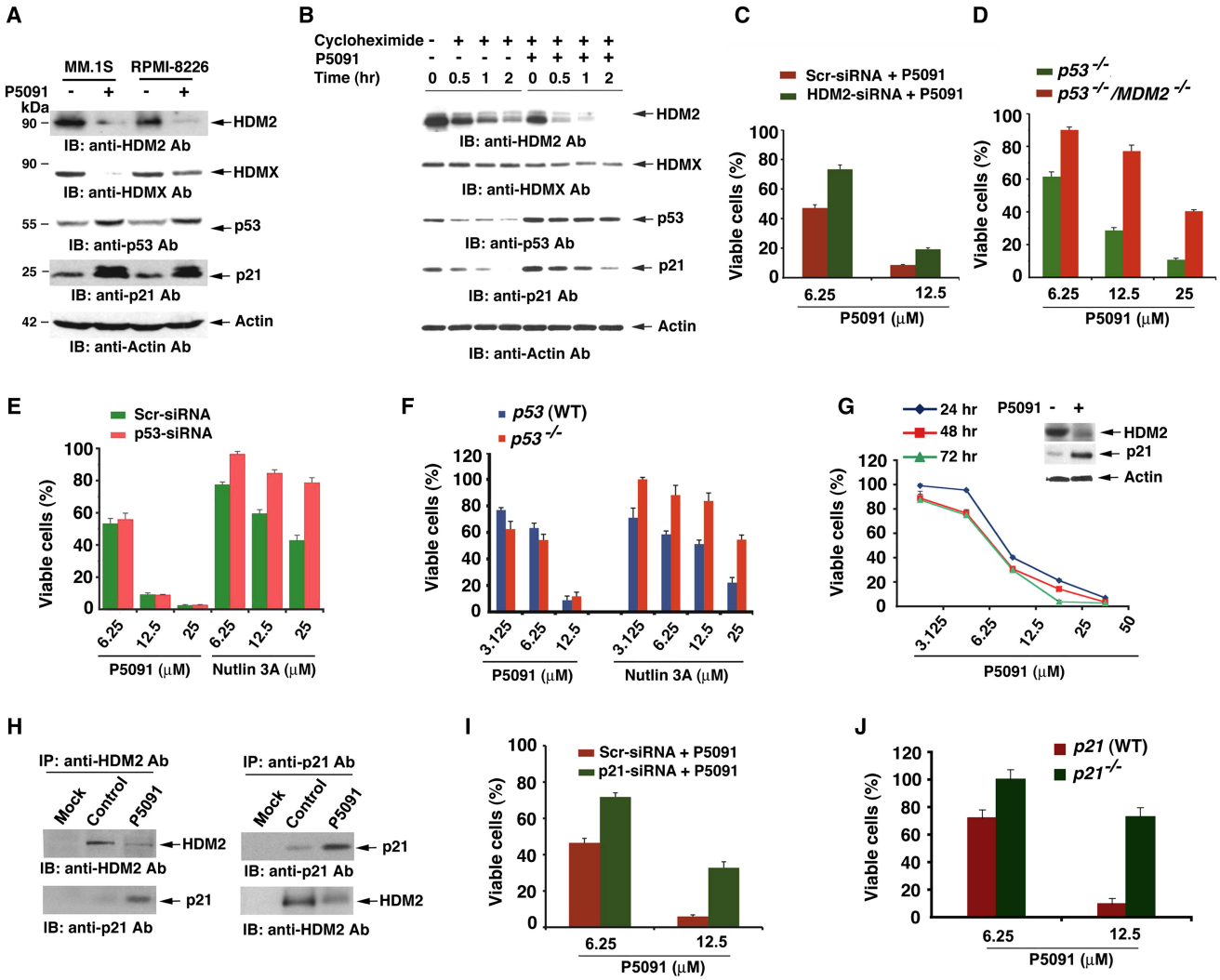

Figure 5. Mechanisms Mediating Anti-MM Activity of P5091

(A) MM.1S and RPMI-8226 cells were treated with P5091 (6.25 and 12.5 μM) for 24 hr; protein lysates were subjected to IB with anti-HDM2, anti-HDMX, anti-p53, anti-p21, or anti-actin antibodies.

(B) MM.1S cells were pretreated with P5091 (6.25 μM) for 4 hr, followed by addition of CHX (50 μg) for the final 0–120 min of the experiment. Protein lysates were subjected to IB using indicated antibodies.

(C) MM.1S cells were transfected with either scr- or HDM2-siRNA. After 24 hr of transfection, cells were treated with vehicle or indicated concentrations of P5091 for an additional 24 hr, followed by analysis of cell viability (mean ± SD; n = 3).

(D) $p53^{-/-}$ and $p53^{-/-}/MDM2^{-/-}$ MEFs were treated with P5091 for 48 hr, followed by analysis of cell viability (mean ± SD; n = 3).

(E) MM.1S cells were transfected with scr- or p53-siRNA, followed by treatment with P5091 or Nutlin-3A for 48 hr, and then analyzed for viability (mean ± SD; n = 3).

(F) HCT116 *p53* (WT) and HCT116 $p53^{-/-}$ cells were treated with DMSO, P5091, or Nutlin-3A for 72 hr, followed by assessment for cell viability (mean ± SD; n = 3).

(G) ARP-1 MM cells were treated with DMSO or P5091 for 48 hr and analyzed for cell viability (mean ± SD; n = 3). Inset: Lysates from control and P5091-treated ARP-1 cells were analyzed for HDM2 and p21 levels using IB.

(H) MM.1S cells were treated with DMSO or P5091 (6.25 μM) for 12 hr; cell lysates were immunoprecipitated with anti-p21, anti-HDM2, or corresponding isotype control (mock) antibodies, and the immune complexes were then subjected to IB with anti-HDM2 and anti-p21 antibodies.

(I) MM.1S cells were transfected with scr- or p21-siRNA, followed by treatment with P5091 for 48 hr, and then analyzed for viability (mean ± SD; n = 3). Percent cell viability was normalized (as 100%) for scr- or p21-siRNA controls, respectively.

(J) HCT116 (WT) and HCT116 $p21^{-/-}$ cells were treated with DMSO or with P5091 for 48 hr, followed by assessment for cell viability (mean ± SD; $p < 0.001$; n = 3).

Error bars in (C–G), (I), and (J) indicate SD. See also Figure S4.

to untreated scr-siRNA, and treatment of HDM2-siRNA transfected cells with P5091 further modestly decreased HDM2 levels (Figure S4D). It is likely that knocking down HDM2 alone negatively impacts the HDM2/HDMX heterocomplex, as well as overall HDM2 E3 ligase activity and polyubiquitylation status of HDM2, thereby resulting in the remaining HDM2 (in HDM2-siRNA cells) being comparatively less sensitive to the effects of P5091. As seen in Figure S4E, which shows absolute levels of viable

cells, the percentage of cell viability in HDM2 knockdown cell is 63.66% (0.322/0.506 × 100%) normalized to scr-siRNA control. Further derivation from absolute values (Figure S4E) show that the percentage of viable cells in scr- and HDM2-siRNA-transfected cells upon treatment with P5091 (6.25 and 12.5 μM) was 47.2%, 8.6%, and 73.3% and 19.2%, respectively (Figure 5C). In concert with these data, P5091 downregulated HDM2 and HDMX, as well as upregulating p53 and p21 levels, in scr-siRNA-transfected cells (Figure S4D). p53 levels were slightly increased by HDM2-siRNA knockdown and further upregulated by P5091 treatment. HDM2-siRNA, like P5091 alone, upregulated p21 levels, which remained unaffected by the combination of HDM2-siRNA and P5091. The role of HDM2 during P5091-induced cell death was further examined using $p53^{-/-}$ and $p53^{-/-}/MDM2^{-/-}$ (double KO) mouse embryonic fibroblasts (MEFs). Results demonstrate significantly reduced cytotoxicity of P5091 in $p53^{-/-}/MDM2^{-/-}$ cells versus $p53^{-/-}$ MEFs (IC_{50} of P5091 for $p53^{-/-}$: 7.72 μM and for $p53^{-/-}/MDM2^{-/-}$: 20.88 μM) (Figure 5D). Together, these data suggest that (1) the effects of HDM2-siRNA alone may not absolutely mimic the responses triggered by P5091 and (2) P5091-induced cytotoxicity is mediated in part via HDM2.

Interestingly, *p53* depletion by siRNA does not affect the P5091-induced decrease in MM.1S cell viability (Figure 5E). In contrast, p53 depletion inhibited cytotoxic effects of Nutlin-3A (Figure 5F), an MDM2-p53 interaction antagonist, suggesting its dependence of p53. We further utilized two different strategies to further address this issue: first, we used HCT116 *p53* (WT) and HCT116 $p53^{-/-}$ cells to show that P5091, but not Nutlin-3A, exerts equipotent cytotoxicity in both cell types (Figure 5F). Second, P5091 treatment decreases the viability of *p53* null ARP-1 MM cells (Figure 5G), associated with decreased HDM2 levels and increased p21 expression (Figure 5G, inset). Together, these data suggest that although P5091 increase p53 levels (Figure 5A), its cytotoxic activity is not dependent on p53. A recent report also highlighted a p53-dependent and p53-independent function of USP7 (Kon et al., 2011). Our findings have important clinical implications because 10%–15% of MM patients have p53 mutations/deletions, which confer drug resistance; a therapeutic approach using USP7 inhibition would allow for potent anti-MM activity, even in this patient population.

Our data show that besides p53, P5091 treatment also upregulates p21, a known downstream target of HDM2-p53 axis (Enge et al., 2009; Vogelstein et al., 2000; Xu et al., 2010). MDM2 inhibition is associated with induction of p21 in human cancer cells regardless of p53 status, suggesting a role of MDM2 in p21 regulation as well as p21 function in mediating p53-independent apoptosis (Wang et al., 2001, 2002; Wu et al., 2002; Zhang et al., 2003, 2004). We examined the effect of P5091 on HDM2-p21 signaling axis. Coimmunoprecipitation assays show that HDM2 is associated with p21 in MM cells and that P5091 downregualates HDM2 and upregualtes p21 (Figure 5H). Silencing of *p21* with siRNA attenuates P5091-induced cytotoxicity (Figure 5I). Similarly, treatment of HCT116 $p21^{-/-}$ cells significantly blocked P5091-triggered cytotoxicity, associated with late-stage apoptosis (Figures 5J and S4F). The P5091-induced increase in p21 protein is in concert with an earlier study showing that MDM2 negatively regulates p21 protein by directly binding to it and facilitating its proteasomal degradation (Zhang et al., 2004). Although P5091 upregulates and stabilizes p21 in MM cells, it triggers a modest accumulation of endogenous ubiquitylated p21 (Figure S4G). The mechanism(s) underlying the USP7-inhibition-mediated p21 ubiquitylation and stabilization in MM cells remains to be defined. Nonetheless, previous reports showed that p21 ubiquitylation is not a prerequisite for proteasomal degradation and that the p21 ubiquitylation may serve some function other than proteasome degradation via conformation changes (Sheaff et al., 2000; Zhang et al., 2004; Xu et al., 2010).

Overall, our mechanistic studies show that (1) P5091-induced cytotoxicity is mediated in part via HDM2-p21 signaling axis and (2) although p53 is upregulated in response to P5091 treatment, the cytotoxic activity of P5091 is not dependent on p53. It is possible that other signaling molecules besides HDM2 or p21 contribute to the overall response to P5091 because HDMX is also the downstream target of USP7 and recent studies showed interaction of USP7 with Claspin, PTEN, or FOXO4.

P5091 Inhibits Human MM Cell Growth In Vivo and Prolongs Survival in the MM.1S MM Xenograft Mouse Model

We next examined the in vivo efficacy of P5091 using human plasmacytoma xenograft and SCID-hu mouse models (Chauhan et al., 2005a). These two distinct models have been immensely useful in extensively validating novel anti-MM therapies bortezomib and lenalidomide, leading to their translation to clinical trials and FDA approval for the treatment of MM. Treatment of MM.1S tumor-bearing mice with intravenous (IV) injection of P5091 inhibits MM tumor growth and prolongs survival of these mice (Figures 6A and 6B). Examination of harvested tumors showed that P5091 inhibited USP7 activity, decreased HDM2, and increased p21 levels relative to tumors from control mice (Figure 6C). P5091 decreases proliferation in harvested tumors, as assessed by BrdU and Ki67 staining (Figures 6D and S5A). P5091 increases the number of cleaved-caspase-3- and TUNEL-positive apoptotic tumor cells versus vehicle treatment (Figures 6E and S5B). P5091 was well tolerated, since no significant weight loss in mice was observed (Figure S5C). These data show potent in vivo apoptotic activity of P5091 against MM cells.

P5091 Triggers Antiangiogenic Activity In Vivo

MM cell growth is associated with angiogenesis, and vascular endothelial growth factor (VEGF) plays a role in this process (Anderson, 2007). To determine whether P5091 triggers antiangiogenic activity, we evaluated tumors harvested from mice by immunostaining using distinct markers of angiogenesis, VEGFR2, and platelet endothelial cell adhesion molecule (PECAM1). P5091 decreases the number of VEGFR2- and PECAM1-positive cells (Figures 6Fa and 6Fb). Tumor sections were also analyzed for expression of LYVE1 (lymphatic vessel marker), ENG (endoglin/CD105), and ACTA2/α-SMA (smooth muscle cell marker). A marked decrease in the number of LYVE1- and ENG-positive cells is observed in tumors from P5091-treated mice versus control mice (Figures 6Fc and 6Fd), suggesting that P5091 exposure results in reduction of tumor vasculature. Dual immunostaining of harvested tumors with PECAM1 and ACTA2 confirms the disappearance of intact larger vessels in P5091-treated

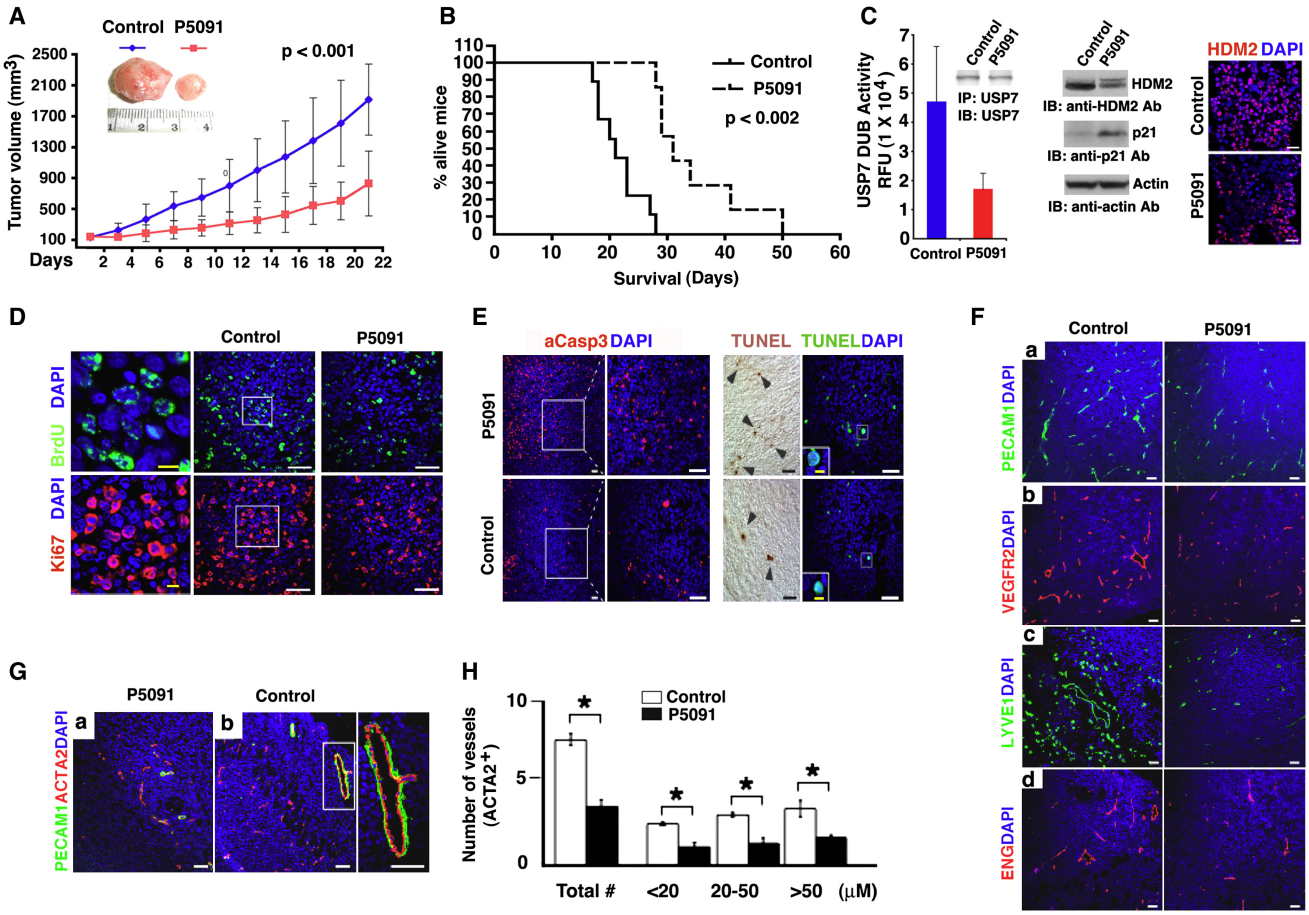

Figure 6. P5091 Inhibits Xenografted Human MM Cell Growth, Prolongs Survival, and Blocks Angiogenesis in CB-17 Mice

(A) Mice bearing human MM.1S MM tumors were treated with vehicle or P5091 (10 mg/kg; IV) twice weekly for 3 consecutive weeks. Data are presented as mean tumor volume ± SD (ten mice/group).

(B) Kaplan-Meier survival plot shows survival of mice.

(C) Tumors from vehicle or P5091-treated mice were analyzed for USP7 activity. Inset: Immunoblot shows equal USP7 protein input. HDM2 and p21 levels in mice tumors were analyzed by IB. Tumor sections from control and P5091-treated mice were immunostained with anti-HDM2 antibody and DAPI. Scale bars, 50 μm.

(D) Tumor sections from control and P5091-treated mice were immunostained with BrdU and Ki67 antibodies. Nuclear staining was performed with DAPI. White rectangle in the middle control panel represents the 5× enlarged area. White scale bars, 50 μm. Yellow scale bars, 10 μm.

(E) Apoptotic cells in tumors sectioned from control or P5091-treated mice were identified by immunostaining for activated caspase-3 (red cells), TUNEL (green cells), and DAPI (blue). White rectangle represents 5× enlarged area. Black arrowheads point at apoptotic cells. Scale bars, 50 μm (10 μm in the inset).

(F) Tumor sections from control and P5091-treated mice were subjected to immunostaining with anti-PECAM1, anti-VEGFR2, anti-LYVE1, or anti-ENG antibodies. Nuclear staining was performed with DAPI. Scale bars, 50 μm.

(G) Tumor sections from control and P5091-treated mice were subjected to dual immunostaining with PECAM1 and ACTA2. White rectangle represents 5× enlarged area. Scale bars, 50 μm.

(H) Quantification of ACTA2-positive cells shown in (G). *p < 0.05.

Error bars represent SD. See also Figure S5.

tumors (Figures 6G and 6H). These data suggest that P5091 inhibits tumor-associated angiogenic activity.

Characterization of P5091 Efficacy in Distinct Animal Models

Because our in vitro data showed that P5091 triggers apoptosis in *p53* null ARP-1 MM cells, we evaluated whether P5091 similarly affects the growth of ARP-1 cells in vivo. Treatment of ARP-1 tumor-bearing mice with P5091 inhibits MM tumor growth and prolongs survival of these mice (Figures 7A and 7B). Importantly, a marked inhibition of USP7 activity was noted in tumors from P5091-treated mice compared with tumors from control mice (Figure 7C). Although P5091 targets USP7, as tested using a panel of DUBs, we cannot rule out the possibility of involvement of yet unknown DUB, other molecules of similar homology, or other USP7 substrates in mediating biological responses. Nonetheless, our data show an early inhibition (at 3 hr) of USP7 activity in vivo in response to P5091 treatment. Blood chemistry profile of P5091-treated mice showed normal levels of bilirubin, hemoglobin, and creatinine (Figure S6A), suggesting that P5091 treatment was well tolerated.

We next compared the in vivo efficacy of P5091 with bortezomib. A head-to-head analysis of P5091 versus bortezomib at their MTD doses showed a similar tumor growth inhibition

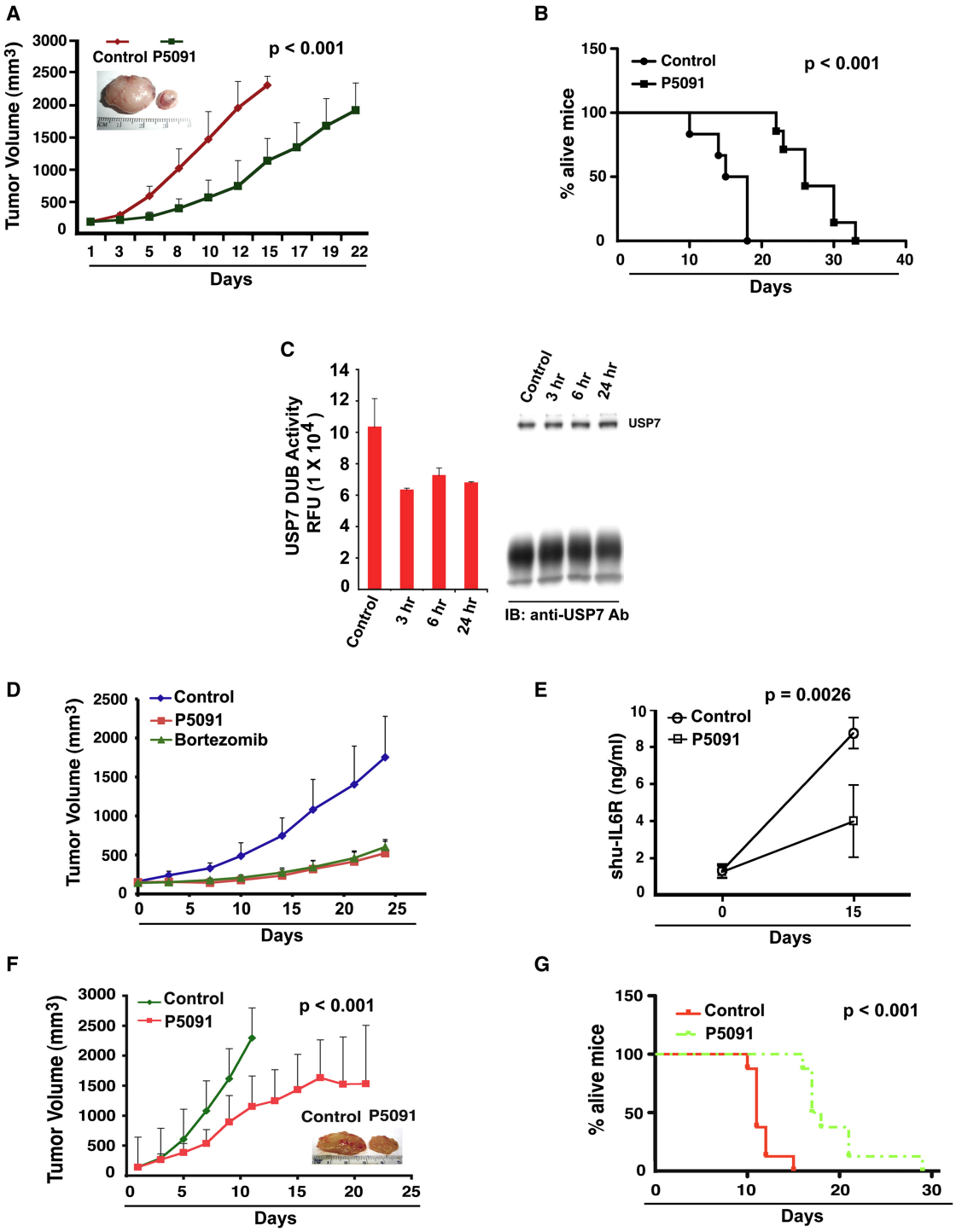

Figure 7. P5091 Targets USP7 In Vivo and Exhibits Antitumor Activity in Distinct Animal Models

(A) Mice bearing human *p53* null ARP-1 MM tumors were treated with either P5091 (10 mg/kg; IV) or vehicle control twice weekly for 3 consecutive weeks. Average and standard deviation of tumor volume (mm^3) is shown from mice versus time when tumor was measured (mean tumor volume ± SD, six mice/group).

(B) Kaplan-Meier plot shows survival in mice.

(C) Tumors from vehicle or P5091-treated mice were analyzed for USP7 activity. Immunoblot shows that equal USP7 protein input.

(D) Average and standard deviation of tumor volume (mm^3) is shown from mice (n = 5/group) versus time when tumor was measured. RPMI-8226 cells (5×10^6 cells/mouse) were implanted in the rear flank of female mice. On day 28–30, mice were randomized to treatment with vehicle, MTD doses of P5091 (20 mg/kg), or with bortezomib (1 mg/kg) on a twice-weekly schedule for 3 weeks.

(E) SCID-hu mice bearing INA-6 MM tumors (five mice/group) were treated with either vehicle alone or P5091 (10 mg/kg), and mouse serum samples were analyzed for shIL-6R.

in RPMI-8266 and MM.1S tumor-bearing mice (Figures 7D and S6B).

Because MM-host BM microenvironment confers growth, survival, and drug resistance in MM cells (Anderson, 2007), we examined whether the anti-MM activity of P5091 is retained in the presence of human BM microenvironment. For these studies, we utilized the SCID-hu model (Anderson, 2007), which recapitulates the human BM milieu in vivo. In this model, INA-6 MM cells are injected directly into human bone chips implanted subcutaneously in SCID mice, and MM cell growth is assessed by serial measurements of circulating levels of soluble human interleukin 6-receptor (shIL-6R) in mouse serum. P5091 treatment inhibited tumor growth in these mice (Figure 7E), suggesting that P5091 can trigger anti-MM activity, even in the presence of the human BM milieu. Finally, in order to determine whether P5091 induces antitumor activity in other cancer cell types, we utilized a human leukemic lymphoblast (CCRF-CEM) xenograft model. Treatment of tumor-bearing mice with P5091 inhibits leukemic tumor growth and prolongs survival of these mice (Figures 7F and 7G), supporting a broad range of antitumor activity of P5091 in cancer types. Together, our data demonstrate that P5091 reduces tumor growth, prolongs survival, and is well tolerated in vivo.

Combined Treatment with P5091 and Lenalidomide, Dex, or the HDAC Inhibitor Induces Synergistic Anti-MM Activity

Our prior preclinical studies (Anderson, 2007) have provided the basis for clinical trials of bortezomib in combination with lenalidomide, Dex, and HDAC inhibitors. Given that P5091, like bortezomib, targets the UPS, we examined whether P5091 similarly enhances the anti-MM activity of other agents. Isobogram analysis (Chou and Talalay, 1984) of synergistic anti-MM activity demonstrated that the combination of low concentrations of P5091 and lenalidomide triggers synergistic anti-MM activity (Figure 8A).

Besides proteasomal degradation, intracellular protein catabolism also occurs via an HDAC-dependent aggressome-autophagic cell death-signaling pathway. Recent clinical trials combining bortezomib and HDAC inhibitor vorinostat (SAHA) show promising outcome in MM. Combination of P5091 and SAHA triggers synergistic anti-MM activity (Figure 8B). These data confirm the potential for clinical trials combining USP7 and HDAC inhibitors. As with lenalidomide and SAHA, the combination of P5091 with conventional anti-MM agent Dex induces synergistic anti-MM activity (Figure 8C). Although definitive evidence of decreased toxicity of combination therapy awaits results of clinical trials, the synergy observed in vitro may allow for use of lower doses and decreased toxicity.

Collectively, our studies utilize MM cell lines, patient tumor cells, and MM xenograft models, as well as biochemical and genetic models, to show the antitumor activity of a USP7 deubiquitylating enzyme inhibitor P5091. The functional specificity of P5091 is confirmed using different strategies: first, cell-free-based experiments using a reporter (Ub-PLA_2)-based assay demonstrate a potent, specific, and selective inhibition of USP7 activity by P5091; second, P5091 enhances degradation of its primary substrate HDM2; third, *USP7* KO in HCT-116 cells confers resistance to P5091; and fourth, P5091 blocks USP7 DUB activity without altering proteasome activity. Treatment of MM cell lines and primary patient MM cells with P5091 inhibits growth and induces apoptosis in tumor cells, including those resistant to conventional and bortezomib therapies, without affecting the viability of normal PBMCs. P5091 triggers apoptosis in MM cells, even in the presence of the MM-host BM microenvironment. Mechanistic studies further show that P5091-triggered apoptosis in MM cells is associated with (1) activation of caspase-8, caspase-9, caspase-3, and PARP and (2) downregulation of USP7 substrate HDM2, as well as increased expression of p53 and p21. Genetic studies using siRNA and KO models show that P5091-induced cytotoxicity is, in part, mediated via HDM2-p21 and occurs independent of p53. In animal tumor model studies, P5091 is well tolerated, inhibits tumor growth, and prolongs survival. Importantly, P5091 inhibits USP7 activity in vivo and induces apoptosis in MM xenografted tumors. Immunostaining of tumor sections shows that antiangiogenic activity contributes to the overall antitumor activity of P5091. A side-by-side efficacy analysis shows a similar antitumor activity of P5091 and bortezomib at their MTD doses. Finally, combining P5091 with lenalidomide, HDAC inhibitor, or Dex induces synergistic anti-MM activity. Our preclinical studies therefore provide the rationale for the development of next-generation UPS-based therapies and specifically demonstrate the promise of therapeutics targeting USP7 to improve patient outcome in MM.

EXPERIMENTAL PROCEDURES

Cell Lines, MM Patient Cells, and Drug Sources

All studies involving human samples were performed under Dana-Farber Cancer Institute IRB committee-approved protocols, through which informed consent was obtained and deidentified samples were utilized. Human MM cell lines MM.1S, MM.1R, RPMI-8226, U266, KMS12PE, ARP-1, INA-6, Dox-40, or LR5 were cultured in RPMI-1640 medium containing 10% fetal bovine serum (FBS) and antibiotics. CCRF-CEM leukemic cells were cultured in 10% FBS and antibiotics. Human colorectal cancer cell lines HCT116 (WT), HCT116 *USP7*$^{-/-}$, HCT116 *p53*$^{-/-}$, and HCT116 *p21*$^{-/-}$ were maintained in McCoy's 5A medium with 10% FBS. Tumor cells from MM patients were purified by $CD138^+$ selection method.

Reagents for In Vitro Enzyme Assays

Recombinant full-length USP5, USP7, and SENP2 catalytic core, as well as amino terminal-tagged hexa His Ub-PLA_2 (Ub-CHOP), Ub-EK_L (Ub-CHOP2), and SUMO3-EK_L(SUMO3-CHOP2), were generated, as previously described (Nicholson et al., 2008; Tian et al., 2011). EK_L was generated by cleaving SUMO3-EK_L with SENP2 core, and mature EK_L was purified by affinity chromatography.

Ubiquitin Protease Assays

Recombinant enzymes in 20 mM Tris-HCl (pH 8.0), 2 mM $CaCl_2$, and 2 mM β-mercaptoethanol were incubated with dose ranges of P5091 for 30 min in a 96-well plate before the addition of Ub-PLA_2 and NBD C_6-HPC (Invitrogen,

(F) Mice bearing CCRF-CEM leukemic tumors were treated with either vehicle or P5091 (10 mg/kg) twice weekly for three consecutive weeks. Data are presented as mean tumor volume ± SD (eight mice/group).
(G) Kaplan-Meier survival plot shows survival of mice.
Error bars indicate SD. See also Figure S6.

A

Combination	P5091 (μM)	P5091 (Fa)	Lenalidomide (μM)	Lenalidomide (Fa)	Fa (com)	CI
1	3	0.7188	1	0.7321	0.4483	0.358
2	3	0.7188	3	0.7166	0.3676	0.265
3	3	0.7188	5	0.5975	0.3049	0.2
4	5	0.5652	1	0.7321	0.3427	0.369
5	5	0.5652	3	0.7166	0.293	0.298
6	5	0.5652	5	0.5975	0.2275	0.212
7	7	0.5256	1	0.7321	0.2532	0.334
8	7	0.5256	3	0.7166	0.2231	0.285
9	7	0.5256	5	0.5975	0.1299	0.149

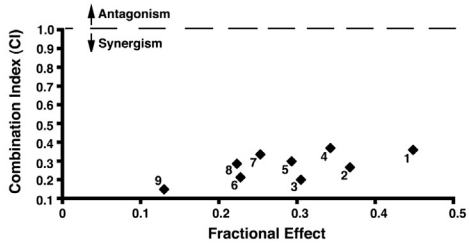

B

Combination	P5091(μM)	P5091 (Fa)	SAHA(nM)	SAHA (Fa)	Fa (com)	CI
1	3	0.7138	80	0.6612	0.4431	0.694
2	3	0.7138	120	0.6137	0.3622	0.601
3	3	0.7138	160	0.515	0.2526	0.409
4	5	0.5611	80	0.6612	0.3513	0.634
5	5	0.5611	120	0.6137	0.2644	0.486
6	5	0.5611	160	0.515	0.2289	0.453
7	7	0.5021	80	0.6612	0.2725	0.559
8	7	0.5021	120	0.6137	0.205	0.432
9	7	0.5021	160	0.515	0.1531	0.333

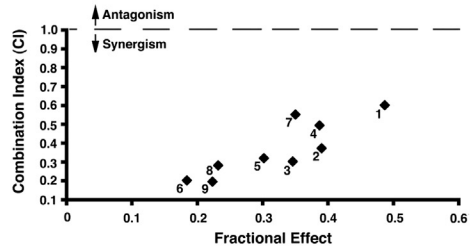

C

Combination	P5091(μM)	P5091 (Fa)	Dex(nM)	Dex (Fa)	Fa (com)	CI
1	3	0.6735	10	0.627	0.487	0.601
2	3	0.6735	20	0.5496	0.39	0.373
3	3	0.6735	30	0.5478	0.346	0.303
4	5	0.561	10	0.627	0.387	0.494
5	5	0.561	20	0.5496	0.302	0.321
6	5	0.561	30	0.5478	0.223	0.196
7	7	0.493	10	0.627	0.35	0.551
8	7	0.493	20	0.5496	0.232	0.282
9	7	0.493	30	0.5478	0.184	0.202

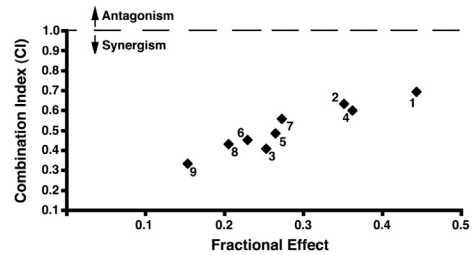

Figure 8. Combination of P5091 and Lenalidomide, SAHA, or Dex Trigger Synergistic Anti-MM Activity

(A) MM.1S cells were treated for 48 hr with P5091, lenalidomide, or P5091 plus lenalidomide and then assessed for viability using MTT assays. Isobologram analysis shows the synergistic cytotoxic effect of P5091 and lenalidomide. The graph (right) is derived from the values given in the table (left). The numbers 1–9 in graph represent combinations shown in the table. FAcom, fraction of viable cells. Combination index (CI) <1 indicates synergy.

(B) MM.1S cells were treated for 48 hr with P5091, SAHA, or P5091 plus SAHA and then assessed for viability using MTT assays. Synergistic anti-MM activity was analyzed as in (A).

(C) MM.1S cells were treated for 48 hr with P5091, Dex, or P5091 plus Dex and then assessed for viability using MTT assays. Synergistic anti-MM activity was analyzed as in (A).

Carlsbad, CA, USA) or Ub-EK_L and EK_L substrate, as previously described (Nicholson et al., 2008; Tian et al., 2011). The liberation of a fluorescent product within the linear range of the assay was monitored using a Perkin Elmer Envision fluorescence plate reader. Vehicle (2% [v/v] DMSO) and 10 mM N-ethylmaleimide (NEM) were included as controls. DUB activity and inhibition assays in living cells were performed as described (Borodovsky et al., 2002).

Ubiquitin-Linked K48 Chain Cleavage Assay

USP7 (30 nM) was preincubated with DMSO or P5091 for 30 min at room temperature (RT) before reaction with polyubiquitin chains for 20 min at 37°C. Samples were resolved by SDS-PAGE and immunoblotted with anti-Ub Ab (Sigma Chemicals, St. Louis, MO, USA).

Human Tumor Xenograft Models

All animal experiments were approved by and conformed to the relevant regulatory standards of the Institutional Animal Care and Use Committee at the Dana-Farber Cancer Institute. For the animal study, P5091 was dissolved in 4% NMP (N-methyl-2-Pyrrolidone), 4% Tween-80, and 92% Milli-Q water at a final concentration of 2 mg/ml. The human plasmacytoma xenograft model was performed as previously described (Chauhan et al., 2008). CB-17 SCID-mice (Charles River Labs, Wilmington, MA, USA) were subcutaneously inoculated with MM.1S, ARP-1, or RPMI-8226 cells in 100 μl of serum-free RPMI-1640 medium. When tumors were measurable (100–180 mm^3), mice were randomized into treatment groups. In the SCID-hu model, human fetal bone grafts were subcutaneously implanted into SCID mice. Four weeks after bone implantation, INA-6 cells were injected directly into the fetal bone implant in SCID mice; as a measure of tumor burden, mouse sera samples were analyzed for shIL-6R by ELISA (R&D Systems, Minneapolis, MN, USA). Upon detection of shIL-6R, mice were treated with vehicle or P5091, and mouse serum was analyzed for alterations in shIL-6R levels.

Statistical Analysis

Statistical significance in drug-treated versus control in vitro cultures, and in tumor xenograft models were determined by using the Student's t test. Survival of mice was measured by using the Prism GraphPad software (Systat Software, San Jose, CA, USA). Isobologram analysis (Chou and Talalay, 1984) was performed using the CalcuSyn software program (Biosoft, Ferguson, MO, USA; Cambridge, UK). A combination index (CI) less than 1.0 indicates synergistic activity.

ACCESSION NUMBERS

The raw data for expression profiling and the CEL files can be found at the Web site Gene Expression Omnibus (http://www.ncbi.nlm.nih.gov/geo/) under accession number GSE39754.

SUPPLEMENTAL INFORMATION

Supplemental Information includes six figures and Supplemental Experimental Procedures and can be found with this article online at http://dx.doi.org/10.1016/j.ccr.2012.08.007.

ACKNOWLEDGMENTS

This investigation was supported by grants from the National Institutes of Health (P50100707, PO1-CA078378, R43DK071391, and R43CA115205). M.A. is supported by VR-2011-2686. K.C.A. is an ACS Clinical Research Professor. D.C. designed research, analyzed data, and wrote the manuscript; Z.T. performed experiments and interpreted data; B.N. designed USP7 activity assay and analyzed data; B.Z. did microscopy; R.C. performed IHC; S.K., C.A.L., J.L.M., M.P.K., M.A., and B.M.K. performed DUB assays; J.W. and W.D.K. synthesized compounds; P.S., S.M., and N.M. analyzed microarray data; M.T. performed animal study; T.H. and P.R. provided clinical samples; and K.C.A. wrote the manuscript. We thank Dr. Bert Vogelstein for HCT116 USP7- and p53-KO cells. We are thankful to Dr. William G. Kaelin (DFCI, Boston, MA) for $p53^{-/-}$ cells and Dr. Guillermina Lozano (M.D. Anderson Cancer Center, Houston, TX) for $p53^{-/-}/MDM2^{-/-}$ cells. B.N., S.K., C.A.L., J.L.M., M.P.K., J.W., and W.D.K. are employees of Progenra, Inc.

Received: October 24, 2011
Revised: May 3, 2012
Accepted: August 9, 2012
Published: September 10, 2012

REFERENCES

Adams, J. (2004). The proteasome: a suitable antineoplastic target. Nat. Rev. Cancer *4*, 349–360.

Anderson, K.C. (2007). Targeted therapy of multiple myeloma based upon tumor-microenvironmental interactions. Exp. Hematol. *35* (4, Suppl 1), 155–162.

Borodovsky, A., Ovaa, H., Kolli, N., Gan-Erdene, T., Wilkinson, K.D., Ploegh, H.L., and Kessler, B.M. (2002). Chemistry-based functional proteomics reveals novel members of the deubiquitinating enzyme family. Chem. Biol. *9*, 1149–1159.

Chauhan, D., Catley, L., Li, G., Podar, K., Hideshima, T., Velankar, M., Mitsiades, C., Mitsiades, N., Yasui, H., Letai, A., et al. (2005a). A novel orally active proteasome inhibitor induces apoptosis in multiple myeloma cells with mechanisms distinct from Bortezomib. Cancer Cell *8*, 407–419.

Chauhan, D., Hideshima, T., and Anderson, K.C. (2005b). Proteasome inhibition in multiple myeloma: therapeutic implication. Annu. Rev. Pharmacol. Toxicol. *45*, 465–476.

Chauhan, D., Singh, A., Brahmandam, M., Podar, K., Hideshima, T., Richardson, P., Munshi, N., Palladino, M.A., and Anderson, K.C. (2008). Combination of proteasome inhibitors bortezomib and NPI-0052 trigger in vivo synergistic cytotoxicity in multiple myeloma. Blood *111*, 1654–1664.

Chou, T.C., and Talalay, P. (1984). Quantitative analysis of dose-effect relationships: the combined effects of multiple drugs or enzyme inhibitors. Adv. Enzyme Regul. *22*, 27–55.

Ciechanover, A. (2005). Proteolysis: from the lysosome to ubiquitin and the proteasome. Nat. Rev. Mol. Cell Biol. *6*, 79–87.

Cummins, J.M., Rago, C., Kohli, M., Kinzler, K.W., Lengauer, C., and Vogelstein, B. (2004). Tumour suppression: disruption of *HAUSP* gene stabilizes p53. Nature *428*, 1 p following 486.

Enge, M., Bao, W., Hedström, E., Jackson, S.P., Moumen, A., and Selivanova, G. (2009). MDM2-dependent downregulation of p21 and hnRNP K provides a switch between apoptosis and growth arrest induced by pharmacologically activated p53. Cancer Cell *15*, 171–183.

Everett, R.D., Meredith, M., Orr, A., Cross, A., Kathoria, M., and Parkinson, J. (1997). A novel ubiquitin-specific protease is dynamically associated with the PML nuclear domain and binds to a herpesvirus regulatory protein. EMBO J. *16*, 1519–1530.

Fang, S., Jensen, J.P., Ludwig, R.L., Vousden, K.H., and Weissman, A.M. (2000). Mdm2 is a RING finger-dependent ubiquitin protein ligase for itself and p53. J. Biol. Chem. *275*, 8945–8951.

Hjerpe, R., Aillet, F., Lopitz-Otsoa, F., Lang, V., England, P., and Rodriguez, M.S. (2009). Efficient protection and isolation of ubiquitylated proteins using tandem ubiquitin-binding entities. EMBO Rep. *10*, 1250–1258.

Hershko, A. (2005). The ubiquitin system for protein degradation and some of its roles in the control of the cell division cycle. Cell Death Differ. *12*, 1191–1197.

Hoeller, D., Hecker, C.M., and Dikic, I. (2006). Ubiquitin and ubiquitin-like proteins in cancer pathogenesis. Nat. Rev. Cancer *6*, 776–788.

Hu, M., Li, P., Li, M., Li, W., Yao, T., Wu, J.W., Gu, W., Cohen, R.E., and Shi, Y. (2002). Crystal structure of a UBP-family deubiquitinating enzyme in isolation and in complex with ubiquitin aldehyde. Cell *111*, 1041–1054.

Itahana, K., Mao, H., Jin, A., Itahana, Y., Clegg, H.V., Lindström, M.S., Bhat, K.P., Godfrey, V.L., Evan, G.I., and Zhang, Y. (2007). Targeted inactivation of Mdm2 RING finger E3 ubiquitin ligase activity in the mouse reveals mechanistic insights into p53 regulation. Cancer Cell *12*, 355–366.

Kon, N., Kobayashi, Y., Li, M., Brooks, C.L., Ludwig, T., and Gu, W. (2010). Inactivation of *HAUSP* in vivo modulates p53 function. Oncogene *29*, 1270–1279.

Kon, N., Zhong, J., Kobayashi, Y., Li, M., Szabolcs, M., Ludwig, T., Canoll, P.D., and Gu, W. (2011). Roles of HAUSP-mediated p53 regulation in central nervous system development. Cell Death Differ. *18*, 1366–1375.

Li, M., and Gu, W. (2011). A critical role for noncoding *5S* rRNA in regulating Mdmx stability. Mol. Cell *43*, 1023–1032.

Li, M., Chen, D., Shiloh, A., Luo, J., Nikolaev, A.Y., Qin, J., and Gu, W. (2002). Deubiquitination of p53 by HAUSP is an important pathway for p53 stabilization. Nature *416*, 648–653.

Li, M., Brooks, C.L., Kon, N., and Gu, W. (2004). A dynamic role of HAUSP in the p53-Mdm2 pathway. Mol. Cell *13*, 879–886.

Lonial, S., Waller, E.K., Richardson, P.G., Jagannath, S., Orlowski, R.Z., Giver, C.R., Jaye, D.L., Francis, D., Giusti, S., Torre, C., et al; SUMMIT/CREST Investigators. (2005). Risk factors and kinetics of thrombocytopenia associated with bortezomib for relapsed, refractory multiple myeloma. Blood *106*, 3777–3784.

Meulmeester, E., Maurice, M.M., Boutell, C., Teunisse, A.F., Ovaa, H., Abraham, T.E., Dirks, R.W., and Jochemsen, A.G. (2005). Loss of HAUSP-mediated deubiquitination contributes to DNA damage-induced destabilization of Hdmx and Hdm2. Mol. Cell *18*, 565–576.

Nicholson, B., Marblestone, J.G., Butt, T.R., and Mattern, M.R. (2007). Deubiquitinating enzymes as novel anticancer targets. Future Oncol. *3*, 191–199.

Nicholson, B., Leach, C.A., Goldenberg, S.J., Francis, D.M., Kodrasov, M.P., Tian, X., Shanks, J., Sterner, D.E., Bernal, A., Mattern, M.R., et al. (2008). Characterization of ubiquitin and ubiquitin-like-protein isopeptidase activities. Protein Sci. *17*, 1035–1043.

Richardson, P.G., Barlogie, B., Berenson, J., Singhal, S., Jagannath, S., Irwin, D., Rajkumar, S.V., Srkalovic, G., Alsina, M., Alexanian, R., et al. (2003). A phase 2 study of bortezomib in relapsed, refractory myeloma. N. Engl. J. Med. *348*, 2609–2617.

Sheaff, R.J., Singer, J.D., Swanger, J., Smitherman, M., Roberts, J.M., and Clurman, B.E. (2000). Proteasomal turnover of p21Cip1 does not require p21Cip1 ubiquitination. Mol. Cell *5*, 403–410.

Song, M.S., Salmena, L., Carracedo, A., Egia, A., Lo-Coco, F., Teruya-Feldstein, J., and Pandolfi, P.P. (2008). The deubiquitinylation and localization of PTEN are regulated by a HAUSP-PML network. Nature *455*, 813–817.

Stommel, J.M., and Wahl, G.M. (2004). Accelerated MDM2 auto-degradation induced by DNA-damage kinases is required for p53 activation. EMBO J. *23*, 1547–1556.

Tian, X., Isamiddinova, N.S., Peroutka, R.J., Goldenberg, S.J., Mattern, M.R., Nicholson, B., and Leach, C. (2011). Characterization of selective ubiquitin and ubiquitin-like protease inhibitors using a fluorescence-based multiplex assay format. Assay Drug Dev. Technol. *9*, 165–173.

Vogelstein, B., Lane, D., and Levine, A.J. (2000). Surfing the p53 network. Nature *408*, 307–310.

Wang, H., Nan, L., Yu, D., Agrawal, S., and Zhang, R. (2001). Antisense anti-MDM2 oligonucleotides as a novel therapeutic approach to human breast cancer: in vitro and in vivo activities and mechanisms. Clin. Cancer Res. *7*, 3613–3624.

Wang, H., Nan, L., Yu, D., Lindsey, J.R., Agrawal, S., and Zhang, R. (2002). Anti-tumor efficacy of a novel antisense anti-MDM2 mixed-backbone oligonucleotide in human colon cancer models: p53-dependent and p53-independent mechanisms. Mol. Med. *8*, 185–199.

Wu, Q., Kirschmeier, P., Hockenberry, T., Yang, T.Y., Brassard, D.L., Wang, L., McClanahan, T., Black, S., Rizzi, G., Musco, M.L., et al. (2002). Transcriptional regulation during p21WAF1/CIP1-induced apoptosis in human ovarian cancer cells. J. Biol. Chem. *277*, 36329–36337.

Xu, H., Zhang, Z., Li, M., and Zhang, R. (2010). MDM2 promotes proteasomal degradation of p21Waf1 via a conformation change. J. Biol. Chem. *285*, 18407–18414.

Zhang, Z., Li, M., Wang, H., Agrawal, S., and Zhang, R. (2003). Antisense therapy targeting MDM2 oncogene in prostate cancer: Effects on proliferation, apoptosis, multiple gene expression, and chemotherapy. Proc. Natl. Acad. Sci. USA *100*, 11636–11641.

Zhang, Z., Wang, H., Li, M., Agrawal, S., Chen, X., and Zhang, R. (2004). MDM2 is a negative regulator of p21WAF1/CIP1, independent of p53. J. Biol. Chem. *279*, 16000–16006.

Zhao, R., Yeung, S.C., Chen, J., Iwakuma, T., Su, C.H., Chen, B., Qu, C., Zhang, F., Chen, Y.T., Lin, Y.L., et al. (2011). Subunit 6 of the COP9 signalosome promotes tumorigenesis in mice through stabilization of MDM2 and is upregulated in human cancers. J. Clin. Invest. *121*, 851–865.